A novel metal flow imaging using electrical capacitance tomography

Thomas Wondrak[1], **Manuchehr Soleimani**[2]

[1] Helmholtz-Zentrum Dresden - Rossendorf, Magnetohydrodynamics, Dresden, 01328, Germany

[2] University of Bath, Department of Electronics & Electrical Engineering, Bath BA2 7AY, United Kingdom

E-mail: t.wondrak@hzdr.de

December 2016

Abstract. The measurement of gas-liquid metal two phase flow is a challenging task due to the opaqueness and the high temperatures. For instance, during continuous casting of steel the distribution of argon gas and liquid steel in the submerged entry nozzle is of high interest, since it influences the quality of the produced steel. In this paper we present the results of a feasibility study for applying the electrical capacitance tomography (ECT) to detect the outer surface of a liquid metal stream. The results of this study are the basis for the development of a new contactless sensor which should be able to detect the outer shape of a liquid metal jet using ECT and the bubbles inside the jet at the same time with mutual inductance tomography.

PACS numbers: 84.37.+q, 06.30 Bp

Keywords: electrical capacitance tomography, liquid metal, surface detection

Submitted to: *Meas. Sci. Technol.*

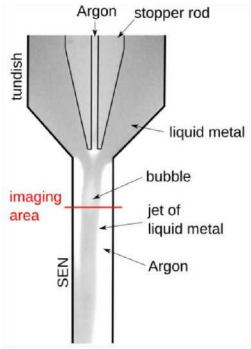

Figure 1. Exemplary x-ray image of the free liquid metal jet in the SEN below the tundish of a model of a continuous caster [8], where slightly below the top of the stopper rod a bubble inside the jet is visible. The desired imaging area of the new combined MIT/ECT sensor is marked by a red line.

1. Introduction

In many metallurgical applications gas is injected into the liquid melt in order to promote mixing or chemical reactions. Typical applications are the cracking of methane and ethane into hydrogen inside a liquid metal reactor [1] or the production of steel where gas is injected at various stages of melt refining, e.g. for carbon reduction or stirring [2]. A very complex two phase flow regime can be found in the submerged entry nozzle (SEN) in a continuous caster. Argon gas is injected into the SEN in order to reduce nozzle clogging and to catch impurities in the melt [3]. Important parameters are the filling degree of the SEN and the bubble distribution in the melt. Since these parameters affect the flow in the mould and the quality of the produced steel, a measurement technique would be highly desirable. Not only the opaqueness of liquid metals, which prevents the use of optical methods, but also the high temperature of liquid steel make great demands on measurement systems.

Beside the use of ultrasound techniques, which can operate in liquids up to 700 °C using acoustic wave guides, for measuring velocity and bubbles [4, 5], neutron [6] or x-ray radiography [7] can be applied to visualise bubbles in liquid metal. Figure 1 shows an x-ray image of a typical flow of liquid metal in the SEN below the stopper rod in a model of a continuous caster available at the Helmholtz-Zentrum Dresden – Rossendorf (HZDR) [8]. The liquid metal leaves the tundish at the bottom and flows into the SEN forming a free jet of liquid metal. The flow rate is controlled by a stopper rod, which also injects Argon gas into the melt through its tip. In this exemplary image a single bubble of Argon is located inside the jet. This method gives a good insight into the two-phase flow in the SEN. However, due to the high attenuation of x-rays in liquid metals, this technique cannot be used in a real caster.

Exploiting the high electrical conductivity of liquid metals, inductive methods such as the mutual inductance tomography (MIT) can be applied at industrial casters. MIT is able to reconstruct the distribution of the electrical conductivity in the cross section of

a pipe. It was already used to visualise the position of the liquid metal strand in the SEN in a real caster [9] and in a cold model [10, 11]. In these model experiments it was shown that the outer surface of the liquid metal strand in the SEN could be reliably detected. However, it was not possible to identify the bubbles inside the liquid jet. Furthermore, the high velocity of about 1.4 m/s of the melt requires a high frame rate of about 140 Hz to visualise bubbles with the size of 10 mm. Due to the nonlinear inverse problem which has to be solved for MIT it is evidently very difficult to reconstruct the surface of the liquid metal column and the bubbles in the melt at the same time. Therefore, we want to combine a single frequency MIT with the electrical capacitance tomography (ECT) in order to use MIT operating with low frequencies for imaging the interior of the liquid metal and ECT for visualising the outer shape of the liquid metal strand. This becomes possible due to the advances of ECT for imaging metallic samples [12].

In this paper we will present a feasibility study for imaging liquid metal using ECT by focusing on stationary experiments. The following challenges have to be considered: First of all, the SEN must consist of insulating material. This is true for continuous casting of steel where the SEN is made of some ceramics (e.g. AlO_3). In some model experiments acrylic glass is used, but for the bigger models the material of the SEN is often stainless steel [13]. In this case the SEN had to be replaced by nonconducting material. Therefore, we will use acrylic glass for the sensor in this feasibility study. Second, it is obvious that even a thin layer of liquid metal at the inner wall of the sensor makes the sensor useless. The forming of such persistent thin liquid films depends on the wettability of the material of the pipe with the liquid metal. Beside this, typically in larger experiments, the liquid metal flows through stainless steel pipes which are usually grounded. In this first feasibility study, we will not investigate this. Last but not least, for the application at steel casters, a sensor for temperatures around 1500 °C has to be build. We believe that this is technically feasible [14].

Taking all these issues into account, we will focus on the detection of the shape of a free liquid metal surface at room temperature using the eutectic alloy GaInSn in floating configuration. Additionally, we will look closer to the effect of a thin film along the inner wall of the sensing area. The issues of grounded liquid metal and high temperatures are left for further investigations.

2. ECT for liquid metal

In this section the forward model of ECT and the inversion method used for metal imaging are described.

2.1. ECT forward model

Electrical Capacitance Tomography (ECT) is a method used for imaging the cross-section of an object. It measures the external capacitance of the bounded object in order to determine the internal permittivity distribution, which is then used to reconstruct an

image of the interior of the object. The ECT mathematical system model can be treated as an electrostatic field problem and hence can be modelled by a Poisson equation (with no free charge this is a Laplace equation) as follows:

$$\nabla \cdot (\varepsilon_r(x,y)\varepsilon_0 \nabla \phi(x,y)) = 0, \tag{1}$$

where ϵ_0 is permittivity of the free space, $\varepsilon_r(x,y)$ is the relative permittivity distribution and $\phi(x,y)$ is the two-dimensional function of the electrical potential distribution. The problem can be discretised by using the Finite Element Method (FEM), such that the mutual capacitance C_{ij} for N-electrode capacitance system (when electrode i is excitation electrode and electrode j is the detector) can be found by:

$$C_{ij} = -\frac{\varepsilon_0}{V_{ij}} \int_{\Gamma_j} \varepsilon_r(x,y) \nabla \phi^i(x,y) \cdot \mathbf{n} d\Gamma_j \qquad \text{for} \quad \begin{cases} i = 1, \ldots, N-1 \\ j = i+1, \ldots, N \end{cases}, \tag{2}$$

where ϕ^i is the potential distribution for the case when electrode i is excitation electrode, V_{ij} is the voltage difference between electrode i and j and $\mathbf{n}$ is a unit vector normal to Γ_j which is the surface of the receiving electrode. For a N-electrode ECT system, $M = N(N-1)/2$ independent measurements can be obtained. To formulate the metal content inside the region of interest in ECT, we represent metallic flow by very high value for dielectric permittivity. These two are equivalent, the electric field inside of metal is zero and electric field inside very high permittivity materials almost zero. To bridge the changes in permittivity distribution and the changes in capacitance measurements, assuming piecewise constant permittivity model with ε_l representing the constant relative permittivity of element l, elements of the jacobian matrix $\mathbf{J}$ can be calculated by:

$$\frac{\partial C_{ij}}{\partial \varepsilon_l} = -\frac{\varepsilon_0}{V_i \cdot V_j} \int_{\Omega} \nabla \phi^i(x,y) \cdot \nabla \phi^j(x,y) dV. \tag{3}$$

V_i and V_j are the voltages of excitation electrodes i and j, respectively.

2.2. The inversion method

The image reconstruction in ECT is an inverse problem, which is an ill-posed nonlinear problem. Therefore, approximation methods based on linearisation are usually used for ECT to solve the inverse problem. A possible general formulation for the regularised inverse problem in the form of unconstrained optimisation problem, is to find the permittivity changes, $\widehat{\Delta\varepsilon_r}$, to minimise the following function:

$$\|\mathbf{J}\Delta\varepsilon_r - \mathbf{m}\|_2^2 + \gamma \,\mathrm{Reg}(\Delta\varepsilon_r), \tag{4}$$

where $\mathbf{m} = \mathbf{C} - \mathbf{C}_0$ is the capacitance change between measurement of test, $\mathbf{C}$ is the real measurement and $\mathbf{C}_0$ is a background measurement, γ is the regularisation factor, $\Delta\varepsilon$ is the change in permittivity distribution, $\mathrm{Reg}(\Delta\varepsilon_r)$ is the stabilising function. One common choice for it is

$$\mathrm{Reg}(\Delta\varepsilon_r) = \|\mathbf{L}(\Delta\varepsilon_r - \overline{\Delta\varepsilon_r})\|_n^n \qquad \infty \geq n \geq 1. \tag{5}$$

$\mathbf{L}$ is the regularisation matrix, $\overline{\Delta\varepsilon_r}$ is the estimated solution of permittivity change from the same reference point. By solving the optimisation equation (4), an explicit solution, denoted by $\widehat{\Delta\varepsilon_r}$, is given by:

$$\widehat{\Delta\varepsilon_r} = (\mathbf{J}^T\mathbf{J} + \gamma\mathbf{L}^T\mathbf{L})^{-1}\mathbf{J}^T\mathbf{m}. \tag{6}$$

However, it is well known that Tikhonov regularisation does not permit sharp edges and only results in smooth edges and oscillations. Therefore, the simplest yet most used form of Tikhonov regularisation is the standard Tikhonov regularisation, which takes $\overline{\Delta\varepsilon_r} = 0$ in equation 5 and giving $\mathbf{L} = \mathbf{I}$, where $\mathbf{I}$ is the identity matrix. In this paper a Laplacian smoothing operator is used for regularisation matrix. ECT image reconstruction for metal flow imaging is highly nonlinear due to the fact that the permittivity of metal flow is indeed equivalent of very high permittivity value. In this study a nonlinear iterative reconstruction approach has been used where the forward operator $\mathbf{F}$ and Jacobian is recalculated in each step:

$$\varepsilon_r^{(k+1)} = \varepsilon_r^{(k)} + (\mathbf{J}^T\mathbf{J} + \gamma\mathbf{L}^T\mathbf{L})^{-1}(\mathbf{J}^T(\mathbf{C} - \mathbf{F}(\varepsilon^{(k)})) - \gamma\mathbf{L}^T\mathbf{L}\varepsilon_r^{(k)}). \tag{7}$$

In each iteration the permittivity image thresholds and a high permittivity of 40 was chosen for metallic region. Regularisation parameters are selected by empirical method. A fixed regularisation value was used in all nonlinear steps. For all computations a two-dimensional model was used.

3. Experimental setup

Figure 2 illustrates a typical ECT system, which consists mainly of three subsystems: the capacitance sensor, data acquisition unit and computer unit. Our capacitance measurement unit is PTL300E, which is a commercial product from process tomography ltd. The signal frequency of the measurement system is 1.25 MHz, i.e., the period of switching is 0.8 μs. This means that it provides enough time for the conductor to reach the electrostatic equilibrium [15]. The effective range of capacitance measurement is from 0.1 fF to 2.0 pF. The sensor consists of 12 electrodes. Figure 3 shows the cross-section of the 12-electrode ECT sensor used in our experiment. The internal radius of the tank is $R_1 = 35$ mm, the external is $R_2 = 40$ mm. The 12 electrodes, each with the width of 16 mm, are evenly distributed on the periphery. Because only stationary experiments were carried out, the measured capacitances were averaged over 60 seconds.

The tank is made of acrylic glass and has a length of 250 mm. On one side the tank is closed and has a removable lid on the opposite side to clean the sensor. Figure 4 shows schematic sketches and photos of the sensor for the two different sensor configurations in horizontal (figure 4(a) and 4(b)) and in vertical (figure 4(c) and 4(d)) arrangement. If the sensor is horizontally aligned, as seen in figures 4(a) and 4(b), different filling levels of the sensing area can be examined. For these experiments a lid (1) with two ports (2) and (3) is mounted on the pipe. The liquid metal is poured into the pipe using port (2) while pressure compensation is accomplished by port (3). On the opposite side (4) the actual level of liquid metal was measured by a ruler. As depicted in figure 4(a) the

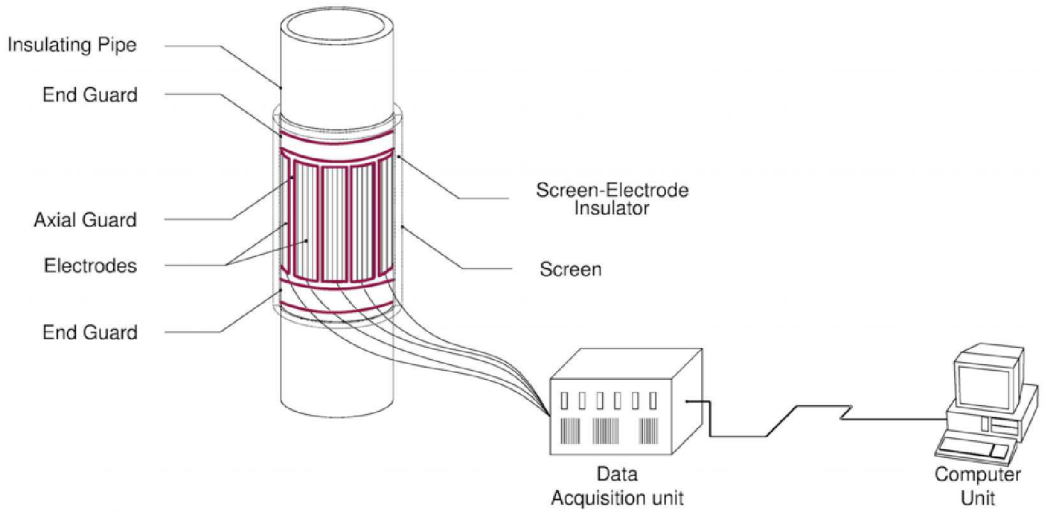

Figure 2. Schematic sketch of a ECT system consisting of a sensor with electrodes, a data acquisition unit and a computer unit

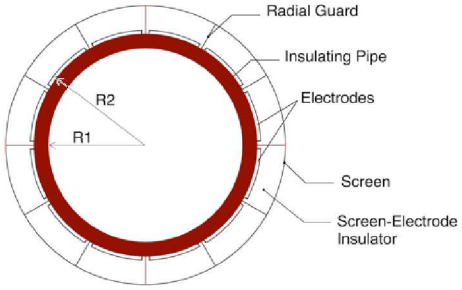

Figure 3. Cross section of the sensing area of the ECT sensor consisting of 12 electrodes, radial guards and the screen

electrode at the top position on the circumference of the lying pipe was sensor number 1.

The sensor can be rotated and set in upright position, as seen in figures 4(c) and 4(d) so that a free falling jet in the sensing area can be produced by pouring liquid metal into the pipe. In order to have a defined radial and azimuthal position of the jet, two lids with ports at different radial positions (6) and (7) are mounted on the sensor. Both lids have an additional port for pressure compensation (8). The ports have a inner diameter of 10 mm and are located at $r_1 = 19\,\mathrm{mm}$ (port (6)) and $r_2 = 17\,\mathrm{mm}$ (port (7)). In this position, we also investigated the wetting conditions.

For the experiments, we used one litre of the eutectic alloy GaInSn which is liquid at room temperature. This simplifies the experimental setup because no heating equipment is required. Additionally, the liquid is neither toxic nor chemically aggressive. The electrical conductivity of GaInSn is 3.3 MS/m.

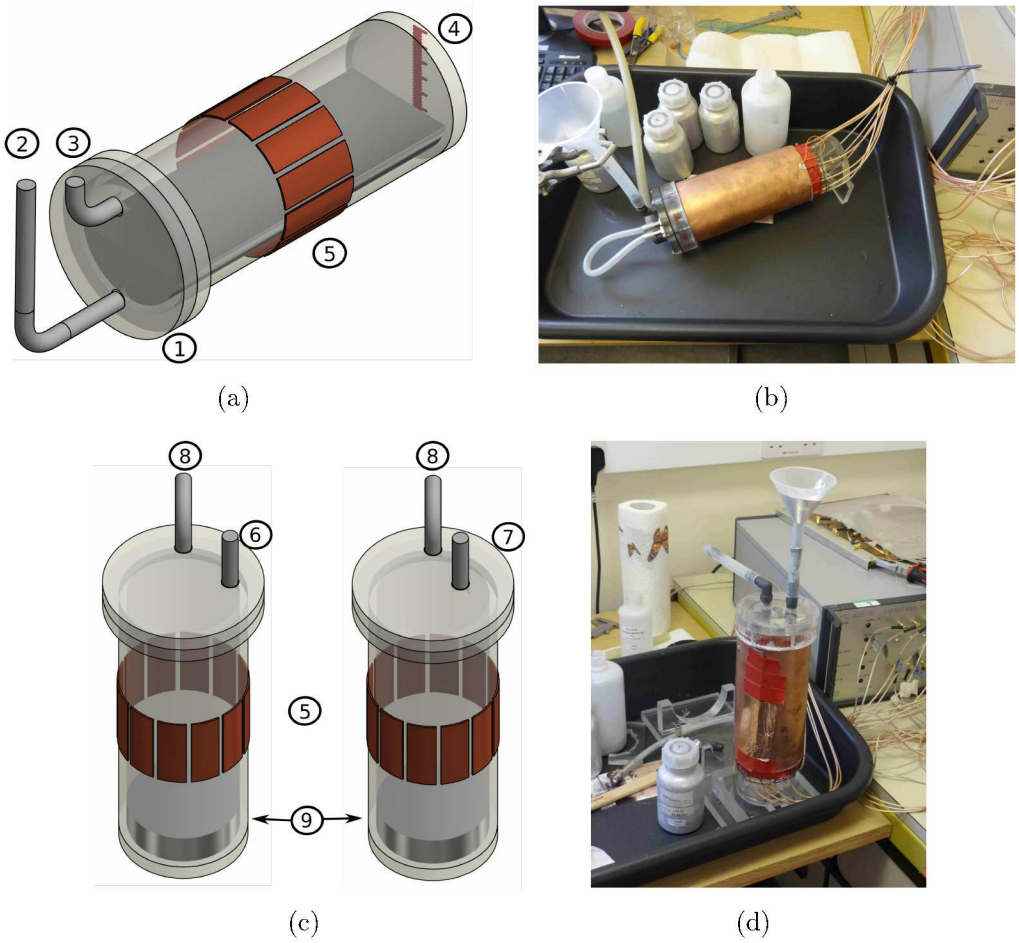

Figure 4. Schematic sketch (a) and photo (b) for the static filling experiments described in section 4.1; removable lid (1) with two ports (2) and (3) for filling the sensor and pressure compensation, respectively, and a ruler (4) for reference level measurement; schematic sketch (c) and photo (d) for the liquid metal jet experiments described in section 4.2; two lids (6),(7) with one port for pouring liquid into it and one port (8) for pressure compensation; liquid metal pool (9)

4. Experiments

In the following section three different experiments are described. In order to test the principal applicability of ECT for measuring liquid metal, the static filling of the cross section of the sensor is tested. In the second experiment, the averaged position over time of a free falling jet of liquid metal is reconstructed. The last experiment investigates the effects of a thin liquid metal film on the inner wall of the sensor.

4.1. Static filling

In the first experiment the reliable detection of the filling of the sensing area with liquid metal was investigated. We used the horizontal arrangement of the sensor as seen in figures 4(a) and 4(b). For each experimental run we first cleaned the sensor

and measured the capacitance of the empty sensor as reference measurement at the beginning. Then, we started to pour liquid metal into the sensor until the level of the liquid metal reached a height of 5 mm. After waiting until the liquid metal was at rest, the capacitance was measured. In the next step the level was increased about 5 mm and the measurement was started again. This procedure was repeated until the sensing area was filled up to 57 mm. Due to the blocking of the outlet with agglomerated oxides, higher levels could not be achieved reliably. In order to fill the sensing area completely, the sensor was tilted by about 25°. Figure 5 shows the reconstructed image of the filling level for all 12 different measurements. The reference level is given by the horizontal black line, which is in good correspondence with the reconstructed levels. After moving the sensor back to its original position, we measured the level of the liquid metal again. As expected, the reconstructed image is similar to the reconstruction depicted in figure 5(k). This indicates that there is no thin layer of liquid metal on the acrylic glass pipe and the acrylic glass pipe was not wetted by the liquid metal. After emptying and opening the sensor, we also checked if a thin film of liquid metal remained on the surface of the sensor. It turned out that it was not the case in this experiment. However, we repeated this experiment several times, and we observed different wetting behaviours after emptying the sensor. In some experiments nearly half of the surface was covered by a liquid metal film. This shows that the wetting could be a random process.

4.2. Liquid metal jet

After showing that ECT is able to reconstruct the shape of a static liquid metal strand, we investigated the case of measuring the average position and the diameter of a free falling jet. For this purpose we moved the sensor in upright position, as seen in figures 4(c) and 4(d), and injected liquid metal through ports (6) and (7) into the empty sensor. The lid could be rotated in arbitrary position in order to place the jet near different electrodes of the ECT system. During pouring of the liquid metal the capacitance was averaged over 60 s. A time dependent measurement with a high frame rate is left for further investigations.

Due to the fact that the centre plane of the sensor is about 125 mm away from the inlet at the lid, neither the position nor the shape of the jet will be the same as at the inlet of the lid. Therefore, by averaging the measurement over 60 s the outer shape of the jet will smear out and the reconstructed diameter of the jet will be greater than defined by the diameter of the inlet. Figure 6 shows the result of three experiments in which the liquid metal was poured into the sensor through ports (6) and (7). The black circle depicts the position and size of the inlet. In figures 6(a) and 6(b) the ports were located near electrode 9. In both measurements the position and the diameter of the reconstructed jet fit quite well to the inlet position. Figure 6(c) shows the reconstructed jet for an experiment in which port (7) was located near electrode 2. In all experiments there is a good agreement regarding the position and the diameter of the jet.

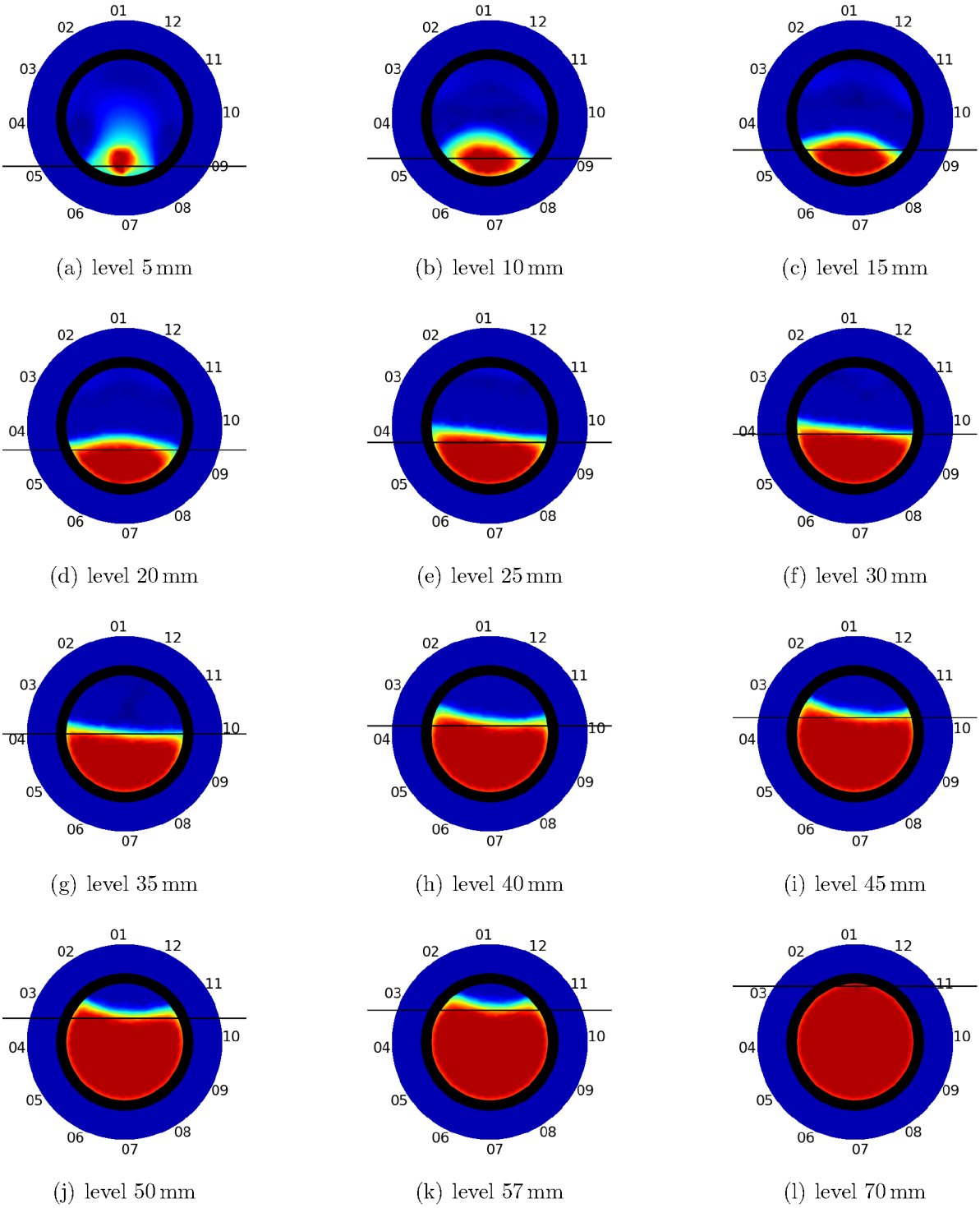

(a) level 5 mm (b) level 10 mm (c) level 15 mm

(d) level 20 mm (e) level 25 mm (f) level 30 mm

(g) level 35 mm (h) level 40 mm (i) level 45 mm

(j) level 50 mm (k) level 57 mm (l) level 70 mm

Figure 5. Reconstructed images for 12 different liquid metal levels in the horizontally aligned pipe, the reference level is indicated by the black horizontal line

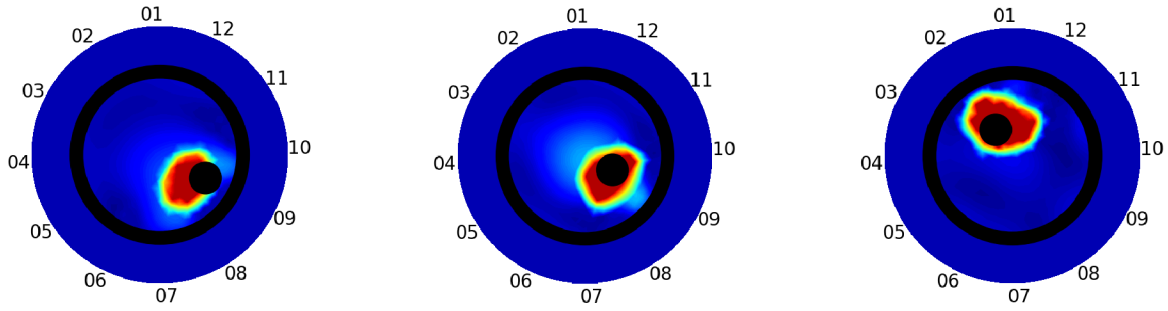

(a) Jet through port (6) at electrode 9

(b) Jet through port (7) at electrode 9

(c) Jet through port (7) at electrode 2

Figure 6. Reconstructed images of the liquid metal jet for 3 different experiments, the black circles indicate the position and the diameter of the inlet port

After each experiment we checked if some droplets are located on the wall. These droplets can be generated, when the liquid metal jet impinges onto the free surface of the liquid metal pool at the bottom of the vessel (see (9) in figure 4(c)). It turned out that during these experiments few very tiny droplets with the size of about 1 mm were left on the wall. These small droplets did not affect the measurement.

4.3. Wetting

For liquid metal ECT the wettability of the wall with the liquid metal plays an important role. If the material of the wall has a good wettability with the liquid metal, then a film of liquid metal can be formed on the wall of the sensor. It is obvious that this makes the sensor useless.

In order to examine the effects of wetting, the sensor was cleaned and some liquid metal was poured over the inner wall of the sensor. Due to the good wettability of acrylic glass and GaInSn a thin film of liquid metal remains on the wall after pouring. Figure 7(a) shows a photo of the partly wetted surface of the sensor with GaInSn. It can clearly be seen that the area between electrode 9 and 7, marked by a red rectangle, is wetted with liquid metal. The according reconstruction is seen in figure 7(b). Figure 7(c) shows a reconstruction where only electrodes 3,2,1,12 are not covered by a thin liquid metal film. It is evident that a thin film of liquid metal makes the sensor useless.

Additionally, we tested several materials, including PVC, PEEK, Teflon and Macor. It turned out that Teflon would be the best choice for a ECT sensor for GaInSn. On this material the liquid metal does not stick to the surface.

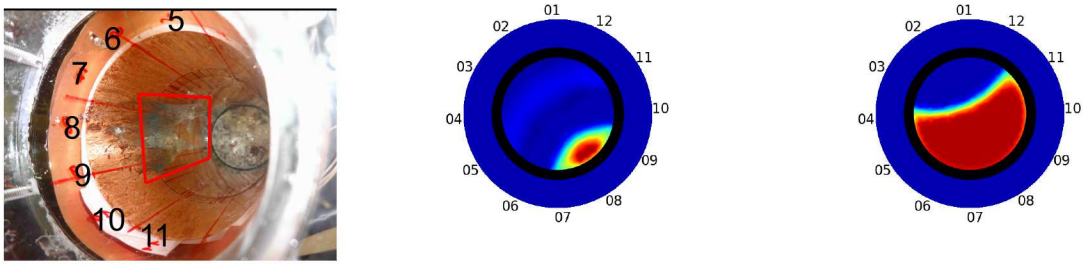

(a) (b) (c)

Figure 7. Photo (a) of a thin liquid metal layer on the inner surface of the sensor between sensor 7 and 9 marked by a red rectangle and the reconstructed image (b) of this experiment; reconstructed image (c) of a second experiment in which only electrodes 3,2,1,12 were not covered by a thin film

5. Conclusion

In this paper we investigated the applicability of ECT for detecting the outer shape of liquid metal jets. The eutectic alloy GaInSn was used which is liquid at room temperature. We were able to reconstruct different levels of liquid metal in the cross section of the sensor. Going towards the detection of the outer surface of the liquid metal jet in the SEN, we set the sensor in upright position and generated a free falling jet of liquid metal in the sensor. It turned out that with this sensor reasonable resolution can be achieved. One important issue for ECT and liquid metal is the formation of a thin liquid metal film on the inner surface of the sensor due to the wettability of the material of the sensor with the liquid metal. It turned out that the surface of the acrylic glass has a good wettability with GaInSn, but it seems to be a random process. Therefore, special care has to be taken to reduce the wettability. This may be achieved by using Teflon for the inner wall of the sensor. The presented results indicate that ECT can be used for the detection of the surface of liquid metal which gives hope that a combined ECT/MIT sensor can also be built.

In order to apply ECT to a continuous steel caster, following issues have to be addressed. Due to the high velocity of about 1 m/s of the liquid metal in the SEN, the frame rate of ECT system has to be increased at least to 100 Hz which is achievable with the most existing ECT systems. Additionally, it has to be checked if ECT measurements are also possible for grounded liquid metals. It is planned to place the electrodes for ECT directly on the outer wall of the SEN which is made of ceramics. The effects of the high temperature of the liquid steel of about 1500 °C on the measurement has to be investigated. Last but not least the wetting conditions of liquid steel on the ceramic walls of the pipe had to be analysed.

Acknowledgments

Financial support of this research by the German Helmholtz Association in the frame of the Helmholtz-Alliance LIMTECH is gratefully acknowledged.

References

[1] M. Seerban, M. Lewis, C. Marshall, and R. Doctor. Hydrogen production by direct contact pyrolysis of natural gas. *Energy Fuels*, 17:705–713, 2003.

[2] C. P. Manning and R. J. Fruehan. Emerging technologies for iron and steelmaking. *JOM*, 53:34–43, 2001.

[3] L. F. Zhang and B. G. Thomas. State of the art in evaluation and control of steel cleanliness. *Iron and Steel Institute of Japan International*, 43(3):271–291, 2003.

[4] Y. Takeda. Development of an ultrasound velocity profile monitor. *Nuclear Engineering and Design*, 126(2):277 – 284, 1991.

[5] A. Andruszkiewicz, K. Eckert, S. Eckert, and S. Odenbach. Gas bubble detection in liquid metals by means of the ultrasound transit-time-technique. *European Physical Journal - Special Topics*, 220:53–62, 2013.

[6] Y. Saito, X. Shen, K. Mishima, and M. Matsubayashi. Shape measurement of bubble in a liquid metal. *Nuclear Instruments and Methods in Physics Research Section A: Accelerators, Spectrometers, Detectors and Associated Equipment*, 605:192 – 196, 2009.

[7] N. Shevchenko, S. Boden, S. Eckert, D. Borin, M. Heinze, and S. Odenbach. Application of X-ray radioscopic methods for characterisation of two-phase phaenomena and solidification processes in metallic melts. *European Physical Journal - Special Topics*, 220:63–77, 2013.

[8] K. Timmel, N. Shevchenko, M. Röder, M. Anderhuber, P. Gardin, S. Eckert, and G. Gerbeth. Visualization of liquid metal two-phase flows in a physical model of the continuous casting process of steel. *Metallurgical and Materials Transactions B*, 46:700–710, 2015.

[9] X.D. Ma, A.J. Peyton, R. Binns, and S.R. Higson. Electromagnetic techniques for imaging the cross-section distribution of molten steel flow in the continuous casting nozzle. *IEEE Sensors Journal*, 5(2):224–232, 2005.

[10] N. Terzija, W. Yin, G. Gerbeth, F. Stefani, K. Timmel, T. Wondrak, and A. J. Peyton. Use of electromagnetic induction tomography for monitoring liquid metal/gas flow regimes on a model of an industrial steel caster. *Measurement Science & Technology*, 22(1):015501, 2011.

[11] T. Wondrak, S. Eckert, G. Gerbeth, K. Klotsche, F. Stefani, K. Timmel, A. J. Peyton, N. Terzija, and W. Yin. Combined electromagnetic tomography for determining two-phase flow characteristics in the submerged entry nozzle and in the mold of a continuous casting model. *Metallurgical and Materials Transactions B*, 42(6):1201–1210, 2011.

[12] M. Zhang and M. Soleimani. Imaging floating metals and dielectric objects using electrical capacitance tomography. *Measurement*, 74:143–149, 2015.

[13] K. Timmel, S. Eckert, G. Gerbeth, F. Stefani, and T. Wondrak. Experimental modeling of the continuous casting process of steel using low melting point metal alloys – the limmcast program. *Iron and Steel Institute of Japan International*, 50:1134–1141, 2010.

[14] S. Liu, Q. Chen, X. Xiong, Z. Zhang, and J. Lei. Preliminary study on ect imaging flames in porous media. *Measurement Science & Technology*, 19:094017, 2008.

[15] Z. Zushou. The time to reach electrostatic equilibrium of a conductor. *Physics and Engineering*, 12:20–21, 2003.